J. Fluid Mech. (2003), *vol.* 492, *pp.* 251–270.
DOI: 10.1017/S0022112003005573 Printed in the United Kingdom

Nonlinear saturation of the Rayleigh instability due to oscillatory flow in a liquid-lined tube

By DAVID HALPERN[1] AND JAMES B. GROTBERG[2]

[1]Department of Mathematics, University of Alabama, Tuscaloosa, AL 35487, USA

[2]Department of Biomedical Engineering, University of Michigan, Ann Arbor, MI 48109, USA

(Received 22 August 2002 and in revised form 8 May 2003)

In this paper, the stability of core–annular flows consisting of two immiscible fluids in a cylindrical tube with circular cross-section is examined. Such flows are important in a wide range of industrial and biomedical applications. For example, in secondary oil recovery, water is pumped into the well to displace the remaining oil. It is also of relevance in the lung, where a thin liquid film coats the inner surface of the small airways of the lungs. In both cases, the flow is influenced by a surface-tension instability, which may induce the breakup of the core fluid into short plugs, reducing the efficiency of the oil recovery, or blocking the passage of air in the lung thus inducing airway closure. We consider the stability of a thin film coating the inner surface of a rigid cylindrical tube with the less viscous fluid in the core. For thick enough films, the Rayleigh instability forms a liquid bulge that can grow to eventually create a plug blocking the tube. The analysis explores the effect of an oscillatory core flow on the interfacial dynamics and particularly the nonlinear stabilization of the bulge. The oscillatory core flow exerts tangential and normal stresses on the interface between the two fluids that are simplified by uncoupling the core and film analyses in the thin-film high-frequency limit of the governing equations. Lubrication theory is used to derive a nonlinear evolution equation for the position of the air–liquid interface which includes the effects of the core flow. It is shown that the core flow can prevent plug formation of the more viscous film layer by nonlinear saturation of the capillary instability. The stabilization mechanism is similar to that of a reversing butter knife, where the core shear wipes the growing liquid bulge back on to the tube wall during the main tidal volume stroke, but allows it to grow back as the stoke and shear turn around. To be successful, the leading film thickness ahead of the bulge must be smaller than the trailing film thickness behind it, a requirement necessitating a large enough core capillary number which promotes a large core shear stress on the interface. The core capillary number is defined to be the ratio of core viscous forces to surface tension forces. When this process is tuned correctly, the two phases balance and there is no net growth of the liquid bulge over one cycle. We find that there is a critical frequency above which plug formation does not occur, and that this critical frequency increases as the tidal volume amplitude of the core flow decreases.

1. Introduction

A perfect core–annular flow (CAF) is an axially symmetric and unidirectional flow in which two immiscible fluids fill a circular pipe and flow along its axis, and where the interface between the annular fluid and the core is a cylindrical surface. Flows of this type are common. Examples include separated flow of steam and water in power

generation facilities, in flow in trickle-bed reactors (Melli *et al.* 1990), and lubricated pipelining of crude viscous oils (Joseph & Renardy 1991). When the oil level in a geological formation falls below a certain critical level, pumping the oil out becomes increasingly difficult. Secondary or tertiary oil recovery methods such as water and/or surfactant flooding are used to dislodge and displace the oil which may be present in the form of long cylindrically shaped slugs. In some instances, the core–annular configuration can break up or rupture resulting in disconnected inclusions of one fluid inside the other (Kouris & Tsamopoulos 2001*b*), which is undesirable in many of these applications.

These types of flow are also found in the lung (Johnson *et al.* 1991; Halpern & Grotberg 1992, 1993*b*; Otis *et al.* 1993) which is comprised of a network of bifurcating airway tubes which are coated with a thin viscous film. Often, especially in the case of disease, the liquid film can form a meniscus which plugs the tube, thus obstructing gas exchange (Macklem, Proctor & Hogg 1970). The formation of the liquid meniscus is due to a capillary driven instability, the Rayleigh instability (Rayleigh 1892*a*), which can cause the lining to close up. In addition, airflow can also be obstructed if the airway tube collapses in on itself (Hughes, Rosenzweig & Kivitz 1970). This occurs when the elastic forces of the tube are not large enough to sustain the negative fluid pressures inside the tube caused by surface-tension, and the tube collapses. Closure of the airway can be due to either, or a combination of, these mechanisms. In any case, the instability is dependent on the surface tension of the liquid lining and the presence, or lack of, surfactants.

When there is no base flow, Hammond (1983) developed a model to study the stability of a thin film lining a rigid tube and solved a nonlinear evolution equation for the interface position, assuming a passive air-core phase. He found that waves initially amplified, but eventually saturated into almost disconnected liquid collars. Gauglitz & Radke (1988) extended Hammond's model by including a more accurate representation for the curvature of the air–liquid interface. They found that if the ratio of film thickness to tube radius, ε, exceeds a certain threshold, $\varepsilon_c \approx 0.12$, closure occurs. Johnson *et al.* (1991) analysed the stability of a viscous annular film, incorporating the full interfacial curvature term and including the effects of inertia. Their results showed that the initial growth rate agreed with the linear stability results of Goren (1962), and their model was able to predict closure for sufficiently thick films. Halpern & Grotberg (1992) extended the approach used by Gauglitz & Radke (1988) to demonstrate how wall compliance can enhance the growth of the interfacial instability and how ε_c is affected by wall properties.

The presence of base flows play an important role in determining the fate of the liquid lining. For steady base flow, there has also been considerable work on CAFs, where the core phase is also in motion. Frenkel *et al.* (1987) derived a weakly nonlinear evolution equation, of the Kuramoto–Sivashinsky (KS) type, for the case where the annular film thickness is much smaller than the core radius, the film and core viscosities are the same, and the disturbances in the core are negligible. In some parameter regimes, the core–annular configuration can break up, resulting in disconnected inclusions of one fluid inside the other. However, they found that for sufficiently strong base flow, the base flow could alter the nonlinear behaviour of the film and prevent rupture from occurring. Theories have also been developed for cases where the ratio of the amplitude of the interfacial waves compared to the film thickness is not small for both horizontal and vertical core–annular flows (Aul & Olbricht 1990; Frenkel & Kerchman 1994; Kerchman & Frenkel 1994; Kouris & Tsamopoulos 2001*b*; Kouris & Tsamopoulos 2002). Highly nonlinear evolution

equations of the Hammond type with additional nonlinearities due to the core and/or gravity reveal events such as 'elastic' collisions between pulses and 'deeply inelastic' coalescences of pulses (Frenkel & Kerchman 1994). A sequence of pulse coalescences can activate the core pinch-off events observed by Aul & Olbricht (1990) for core–annular film flows with even very thin films, which were much thinner than in the limiting case of no mean flow (Gauglitz & Radke 1988; Cassidy *et al.* 1999; Halpern & Grotberg 1993*b*). Kouris & Tsamopoulos 2001*a*, and Wei & Rumschitzki 2002*a*, *b* have considered more realistic pore geometries in regard to, for example, oil recovery, by examining the effect of periodic wall constrictions on core–annular flows.

Time periodic two-phase flows have been shown to be both stabilizing and destabilizing. Coward & Papageorgiou (1994) analysed two-phase Couette flow between two plates, where one of the plates moves with a velocity that consists of a steady part combined with an oscillatory component. The interface between the two layers is unstable if the thinner of the two layers contains the more viscous fluid in the case of steady Couette flow (Yih 1967). They showed, using Floquet theory, that this system can be stabilized if the amplitude of the oscillatory component is sufficiently large. Recently, Coward, Papageorgiou & Smyrlis (1995) added a small oscillatory component to the core–annular flow, and obtained a KS equation with the coefficient of the nonlinear term consisting of a constant and a smaller oscillatory part. Halpern & Frenkel (2001) considered the stability of a two-fluid system between horizontal plates with the upper plate oscillating with zero mean velocity, consisting of a thin viscous film which is bounded below by the stationary plate and above by a denser fluid. As in Coward *et al.* (1995), a modified Kuramoto–Sivashinsky equation with an oscillatory nonlinearity was derived for the limiting case of small interfacial deflections. It was found that oscillatory flow could stabilize the Rayleigh–Taylor instability. Increasing the frequency reduces the maximum amplitude of the disturbance since the fraction of the cycle during which the destabilizing effect dominates is curtailed. However, above a certain critical value, which depends on the size of the computational domain, the time asymptotic solution of the modified KS equation changes qualitatively to a profile whose amplitude increases with frequency.

Imposed external oscillations have also been investigated in oil recovery (Graham & Higdon 2002), in reducing breathlessness and carbon dioxide levels in patients with obstructive airway disease, chest wall vibrators may be placed around the patients rib cage, which oscillate at frequencies up to 100 Hz (Edo *et al.* 1998), and in annular extrusion methods for the manufacturing of small hollow fibres (Isayev, Wong & Zeng 1990; Wong, Chen & Isayev 1990). In the manufacturing of optical fibres, an inner plug core of liquid and an outer annulus of a different liquid are co-extruded simultaneously, one around the other. It is important to have a smooth interface between the materials so that the desired mechanical and optical properties are achieved. Instabilities of this interface during concentric co-extrusion have been examined by Chen (1991).

In this paper, we consider the nonlinear instability of a thin film coating the inner surface of a rigid tube. Lubrication theory is used to derive a nonlinear evolution equation for the position of the air–liquid interface. The effect of an imposed oscillatory core flow is explored by assuming, to a first approximation, an uncoupled core-film problem. In § 2, we provide a description of the model equations. The evolution equation for the air–liquid interface is derived in § 3. Linear stability is briefly discussed in § 4. Results of numerical simulations are given in § 5, and conclusions in § 6.

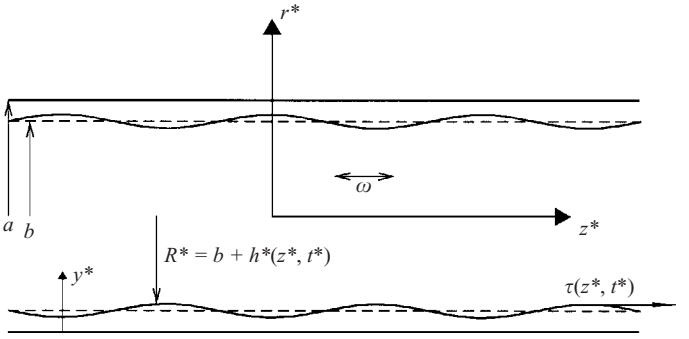

FIGURE 1. Variables describing the film geometry. A cylindrical tube of radius a is coated with a film of thickness $a-b$. The position of the air–liquid interface is at $R^* = b + h^*(z^*, t^*)$ after it has been perturbed.

2. Basic model and scaling

The model is formulated in accordance with the analysis developed by Halpern & Grotberg (1992); however, the present model incorporates the effects of an imposed oscillation in the core fluid and assumes the tube to be a rigid circular cylinder. The flows in the film and the core are governed by the continuity and Navier–Stokes equations, together with interfacial boundary conditions, which are given below.

2.1. *Governing equations in the film region*

Consider a cylindrical tube of radius a, with a uniform liquid film of thickness $a-b$ coating the inside and an air-filled core (see figure 1). In the film, the axial coordinate is scaled with respect to the tube radius, so that $z = z^*/a$ where a starred variable refers to a dimensional quantity. A radial coordinate radial coordinate $y = 1 - \varepsilon r^*/a$, defining the wall at $y = 0$, is introduced, where $\varepsilon = 1 - b/a \ll 1$ is the dimensionless unperturbed film thickness. The radial and axial velocity components are scaled as $(u_f, w_f) = (u^*/(\varepsilon U_{cap}), w^*/U_{cap})$ where $U_{cap} = \varepsilon^3\sigma/\mu_f$ is a capillary velocity (Halpern & Grotberg 1992), time is scaled as $t = t^*/(a/U_{cap})$ and pressure as $p_f = p^*/(\varepsilon\sigma/a)$. The remaining parameters are the constant surface tension of the interface σ, and the fluid viscosity μ_f. To investigate the stability of the film, we perturb the position of the air–liquid interface axisymmetrically to induce a flow within the film. At time t, the interface position is $R(z,t) = (1-\varepsilon) + \varepsilon h(z,t)$ where $h = h^*/(a-b)$ is the deflection of the interface scaled on the unperturbed film thickness.

The mass continuity equation becomes, with these scalings,

$$\frac{\partial w_f}{\partial z} - \frac{1}{1-\varepsilon y}\frac{\partial}{\partial y}((1-\varepsilon y)u_f) = 0, \tag{1}$$

and the radial (r) and axial (z) momentum equations are, respectively,

$$\varepsilon^2 Re_f\left[\frac{\partial u_f}{\partial t} - \frac{u_f}{1-\varepsilon y}\frac{\partial}{\partial y}((1-\varepsilon y)u_f) + w_f\frac{\partial u_f}{\partial z}\right] = \frac{1}{\varepsilon^2}\frac{\partial p_f}{\partial y} + \frac{1}{(1-\varepsilon y)}\frac{\partial}{\partial y}\left((1-\varepsilon y)\frac{\partial u_f}{\partial y}\right) + \frac{\partial^2 u_f}{\partial z^2}, \tag{2}$$

$$\varepsilon^2 Re_f\left[\frac{\partial w_f}{\partial t}-\frac{u_f}{(1-\varepsilon y)}\frac{\partial}{\partial y}((1-\varepsilon y)w_f)+w_f\frac{\partial w_f}{\partial z}\right] = -\frac{\partial p_f}{\partial z}+\frac{1}{(1-\varepsilon y)}\frac{\partial}{\partial y}\left((1-\varepsilon y)\frac{\partial w_f}{\partial y}\right)+\varepsilon^2\frac{\partial^2 w_f}{\partial z^2}, \quad (3)$$

where $Re_f=\rho_f U_{cap}a/\mu_f=\varepsilon^3\rho_f\sigma a/\mu_f^2$ is the film Reynolds number.

2.2. *Governing equations in the core region*

The core fluid oscillates as a result of an imposed time-dependent axial flow rate Q^* of the form

$$Q^*=\tfrac{1}{2}V_T\omega\sin(\omega t_c^*+\varphi),$$

where $\omega=2\pi f$ is the angular frequency of oscillation, V_T is the tidal volume which is equal to the volume of fluid displaced, and φ is a non-zero phase angle. In the present model, the velocity scale for the core flow $U_c=\omega L_T$ is assumed to be large compared to that for the film, U_{cap}, where $L_T=V_T/(\pi b^2)$ is the stroke length. Because of this large discrepancy in velocity scales, it is helpful to use a different set of scales for the core problem. The governing equations in the core are non-dimensionalized using the following scalings: the time, $t_c=\omega t_c^*$; the radial coordinate $r_c=r_c^*/b$; the axial coordinate, $z_c=\delta z_c^*/b$ where $\delta=b/L$; $p_c=\delta b p_c^*/\mu_a U_c$; and the velocities $(u_c, w_c)=(u_c^*/\delta U_c, w_c^*/U_c)$ where L is a characteristic axial length scale for the core flow, which is taken to be the tube length, such that $\delta\ll 1$. The core pressure gradient is of the form

$$\frac{\partial p_c}{\partial z_c}=B(z_c)\sin t_c, \quad (4)$$

and the continuity and axial and radial momentum equations become

$$\frac{1}{r_c}\frac{\partial}{\partial r_c}(r_c u_c)+\frac{\partial w_c}{\partial z_c}=0, \quad (5)$$

$$\alpha^2\frac{\partial w_c}{\partial t_c}+\alpha^2\delta\lambda\left(w_c\frac{\partial w_c}{\partial z_c}+u_c\frac{\partial w_c}{\partial r_c}\right)=-B\sin t_c+\frac{1}{r_c}\frac{\partial}{\partial r_c}\left(r_c\frac{\partial w_c}{\partial r_c}\right)+\delta^2\frac{\partial^2 w_c}{\partial z_c^2}, \quad (6)$$

$$\alpha^2\delta\frac{\partial u_c}{\partial t_c}+\alpha^2\delta^2\lambda\left(w_c\frac{\partial u_c}{\partial z_c}+u_c\frac{\partial u_c}{\partial r_c}\right)=-\frac{1}{\delta}\frac{\partial p_c}{\partial r_c}+\delta\left(\delta^2\frac{\partial^2 u_c}{\partial z_c^2}+\frac{\partial}{\partial r_c}\left(\frac{1}{r_c}\left(\frac{\partial}{\partial r_c}(r_c u_c)\right)\right)\right), \quad (7)$$

where $\alpha=(\rho_c\omega/\mu_c)^{1/2}b$ is the core Womersley number, the ratio of inertia forces due to the oscillatory motion to viscous forces, $\lambda=L_T/b$ is the ratio of stroke length to the average tube radius, and ρ_c is the core fluid density.

2.3. *Boundary conditions*

No-slip and no-penetration boundary conditions are applied at the tube wall ($r=1$), so that

$$w_f(r=1, z, t)=u_f(r=1, z, t)=0. \quad (8)$$

At the core–film interface, we apply kinematic boundary conditions and boundary conditions derived from continuity of tangential and normal stresses. The kinematic

boundary condition is a consequence of the interface at $r = R(z,t) = 1 - \varepsilon + \varepsilon h(z,t)$ (or $r_c = R_c(z_c, t_c)$), being a material surface moving with the local fluid velocity. It can either be written in terms of the film or core variables:

$$\frac{\partial h}{\partial t} = u_f - w_f \frac{\partial h}{\partial z} \quad \text{or} \quad \frac{\partial R_c}{\partial t_c} = \delta \left(u_c - w_c \frac{\partial R_c}{\partial z_c} \right) \quad \text{at} \quad r = R. \tag{9}$$

The other boundary conditions at the interface are continuity of velocity $[\boldsymbol{u}_j^*] = 0$, continuity of tangential stress $[\boldsymbol{\tau}_j^* \cdot \boldsymbol{t}] = 0$ and a jump in normal stress condition due to surface tension σ $[\boldsymbol{\tau}_j^* \cdot \boldsymbol{n}] = \sigma K \boldsymbol{n}$, where $[\boldsymbol{x}]$ denotes the jump in $\boldsymbol{x}$ across the air–liquid interface, the subscript j stands either for c (the core) or for f (the film), $\boldsymbol{t}$ and $\boldsymbol{n}$ are the unit tangent and normal vectors to the interface, ∇_s is the surface gradient operator, $K = -\nabla_s^* \cdot \boldsymbol{n}$ is the interfacial curvature and $\boldsymbol{\tau}_j^* = S_j^* \cdot \boldsymbol{n}$ is the stress vector and $S_j^* = -I p_j^* + \mu_j (\nabla \boldsymbol{u}_j^* + \nabla \boldsymbol{u}_f^{*T})$ is the stress tensor. In dimensionless form, the velocity, tangential stress and normal stress conditions are given by

$$w_c = \frac{1}{(1-\varepsilon)\lambda\Omega} w_f, \quad u_c = \frac{\varepsilon}{\delta} \frac{1}{(1-\varepsilon)\lambda\Omega} u_f, \tag{10}$$

$$\frac{\partial w_f}{\partial y} - \varepsilon^2 \frac{\partial u_f}{\partial z} - \frac{2\varepsilon^2 h_z}{1 - \varepsilon^2 h_z^2} \left(\frac{\partial w_f}{\partial z} + \frac{\partial u_f}{\partial y} \right) + \frac{Ca}{1-\varepsilon} \left(\frac{\partial w_c}{\partial r_c} + \delta^2 \frac{\partial u_c}{\partial z_c} - 2\delta^2 \frac{R_{cz_c}}{1 - \delta^2 R_{cz_c}^2} \left(\frac{\partial w_c}{\partial z_c} - \frac{\partial u_c}{\partial r_c} \right) \right) = 0, \tag{11}$$

and

$$\begin{aligned} &-p_f + \frac{2\varepsilon^2}{1+\varepsilon^2 h_z^2} \left(-\frac{\partial u_f}{\partial y} - h_z \left(\varepsilon \frac{\partial u_f}{\partial z} + \frac{\partial w_f}{\partial y} \right) - \varepsilon^2 h_z^2 \frac{\partial w_f}{\partial z} \right) \\ &- \frac{\varepsilon}{1-\varepsilon} Ca \left(-\frac{1}{\delta} p_c + 2\delta \frac{1}{1 + \delta^2 R_{cz_c}^2} \left(\frac{\partial u_c}{\partial r_c} - R_{cz_c} \left(\frac{\partial u_c}{\partial z_c} + \frac{\partial w_c}{\partial r_c} \right) - \delta^2 R_{cz_c}^2 \frac{\partial w_c}{\partial z_c} \right) \right) \\ &= -\left(\frac{1}{\left(1+\varepsilon^2 h_z^2\right)^{1/2}} \frac{h}{(1-\varepsilon)(1-\varepsilon+\varepsilon h)} + \frac{h_{zz}}{\left(1+\varepsilon^2 h_z^2\right)^{3/2}} \right. \\ &\left. - \frac{\varepsilon}{1-\varepsilon} \frac{h_z^2}{\left(1+\varepsilon^2 h_z^2\right)\left(1 + \left(1+\varepsilon^2 h_z^2\right)^{-1/2}\right)} \right), \end{aligned} \tag{12}$$

where $\Omega = \omega a / U_{cap}$ is a dimensionless frequency representing the ratio of the capillary time scale to the oscillatory core time scale, and $Ca = \mu_c \omega L_T / (\varepsilon^2 \sigma)$ is the core capillary number.

3. The thin-film high-frequency limit

We consider the limit $\varepsilon \ll 1$ for thin films, which simplifies many of the above expressions in a lubrication approximation. One of the effects is to cause $1/\Omega \ll 1$, that is the characteristic core time scale $1/\omega$, is much shorter than the characteristic capillary time scale of the film a/U_{cap}. Then, the effects of an oscillatory core flow on the stability of the film can be modelled by considering an uncoupled problem, where the low-viscosity core fluid perceives the thin highly viscous film as a rigid boundary.

Assuming $1/\Omega = O(\varepsilon)$, the continuity of velocity boundary condition, equation (10), reduces to a no-relative-slip condition at leading order for the core fluid:

$$w_c = 0, \quad u_c = 0, \tag{13}$$

provided $1/\Omega\lambda \ll 1$. The terms of order ε, δ and higher that appear in the tangential stress condition, equation (11), can be neglected in the limit of $(\varepsilon, \delta) \to (0, 0)$, so that, at leading order, we obtain the following expression for the shear stress τ at the interface:

$$\tau = \frac{\partial w_f}{\partial y} = -\frac{Ca}{1-\varepsilon}\frac{\partial w_c}{\partial r_c}. \tag{14}$$

The viscous terms in the normal stress condition are dropped since the film viscous terms are of order ε^2 and the core viscous terms are order δ smaller than the leading-order tangential stress kept in (14). However, we use an approximation for the curvature due to Gauglitz & Radke (1988) which retains some higher-order terms in ε. Equation (12) then becomes

$$p_f - \frac{\varepsilon}{\delta}\frac{Ca}{1-\varepsilon}P_c = \left(\frac{h}{(1-\varepsilon)(1-\varepsilon+\varepsilon h)} + h_{zz}\right). \tag{15}$$

The kinematic boundary condition, equation (9), makes R_c independent of the fast time scale since from (13) the core velocity at the interface is zero. Thus, the characteristic core time scale $1/\omega$, is much shorter than the characteristic capillary time scale of the film a/U_{cap} and we achieve a quasi-steady analysis for the core flow dynamics in terms of its dependence on the interfacial position.

3.1. *Evolution equation for interface deflection*

An evolution equation for the deflection of the interface can be accomplished by making the further approximation that $\varepsilon^2 Re_f \ll 1$. This enables us to use lubrication theory and express the velocity field in the film region in terms of $h(z, t)$. The governing equations (1)–(3) then reduce, respectively, to,

$$\frac{1}{1-\varepsilon y}\frac{\partial}{\partial y}((1-\varepsilon y)u_f) - \frac{\partial w_f}{\partial z} = 0, \tag{16}$$

$$\frac{\partial p_f}{\partial y} = 0 + O(\varepsilon^2), \tag{17}$$

and

$$\frac{\partial^2 w_f}{\partial y^2} = \frac{\partial p_f}{\partial z} + O(\varepsilon). \tag{18}$$

Note that as in Gauglitz & Radke (1988), equation (16) is the exact continuity equation. At the liquid–wall interface, $y = 0$, we impose the no-slip and no-penetration boundary condition, equation (8), and at the liquid–air interface $y = 1 - h(z, t)$, we apply the tangential stress and normal stress boundary conditions, equtions (14) and (15). The axial component of velocity is obtained by integrating (18):

$$w_f = \frac{\partial p_f}{\partial z}\left[\frac{y^2 - 2y(1-h)}{2}\right] - \tau y, \tag{19}$$

where p_f is given by (15) and τ by (14). Applying the kinematic condition on the air–liquid interface at $y = 1 - h$, gives,

$$\frac{\partial h}{\partial t} - u_f(y = 1-h, z, t) + w_f(y = 1-h, z, t)\frac{\partial h}{\partial z} = 0, \tag{20}$$

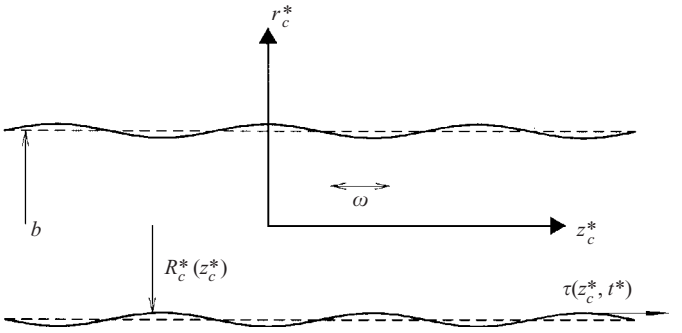

FIGURE 2. Variables describing the oscillatory core flow driven at frequency ω in a wavy dry tube of mean radius b. The radial position of the wall is given by $r_c^* = R(z_c^*)$ where z_c^* is the axial coordinate. $\tau^*(z_c^*, t^*)$ is the shear-stress on the wavy boundary.

where $u_f(y = 1-h, z, t)$ is the radial velocity component evaluated at the air–liquid interface, obtained from the continuity equation, (16):

$$u_f(y=1-h,z,t) = \frac{1}{1-\varepsilon(1-h)} \int_0^{1-h} (1-\varepsilon y) \frac{\partial w_f}{\partial z}\, \mathrm{d}y. \tag{21}$$

The kinematic condition, equation (20), then simplifies to

$$\frac{\partial h}{\partial t} = -\frac{1}{3(1-\varepsilon+\varepsilon h)} \frac{\partial}{\partial z} \left(\frac{\partial p_f}{\partial z}(1-h)^3 + \tfrac{3}{2}\tau(1-h)^2 \right), \tag{22}$$

which agrees with the model by Halpern & Grotberg (1992) when the core flow is turned off, i.e. $\tau = 0$ and $p_c = 0$.

The shear stress τ function that appears in (22) depends on the core flow, which is solved in the next section.

3.2. *The core region*

In the limit of thin highly viscous films and high frequency, the core fluid perceives the air–liquid interface as a dry rigid tube whose boundary is wavy having average radius, b, and a deflection from the mean of order ε, and characteristic axial scale, L (see figure 2). This is a consequence of obtaining the no-slip and no-penetration boundary conditions, equation (13), at $r_c = R_c(z_c)$. The aim is to find an estimate for the shear stresses, τ, and pressure fluctuations, p_c, that will be applied to the deforming air–liquid interface of the closure problem. A small-slope approximation is applied to the momentum equations, (6) and (7), since the interfacial deflection is of order εb, which is smaller than the axial scale L. Thus, the axial derivative $\partial/\partial z_c$ is of order ε. By also assuming that $\varepsilon\alpha^2\delta\lambda \ll 1$, the convective acceleration terms in the momentum equations can be neglected. Equation (7) then implies that the core pressure is independent of the radial coordinate. The axial momentum equation, (6), can also be simplified, reducing to

$$\alpha^2 \frac{\partial w_c}{\partial t_c} = -B \sin t_c + \frac{1}{r_c} \frac{\partial}{\partial r_c} \left(r_c \frac{\partial w_c}{\partial r_c} \right),$$

where we have assumed that α can be of order one. This equation can be integrated

to yield the axial component of velocity

$$w_c(r_c, z_c, t_c) = \mathrm{Re}\left(\frac{\mathrm{i}B(z_c)}{\alpha^2}\left(1 - \frac{J_0(\kappa_c r_c)}{J_0(\kappa_c R_c(z_c))}\right)\exp(\mathrm{i}(t_c - \pi/2))\right) \tag{23}$$

where Re denotes the real part of a complex function, J_0 is the zeroth-order Bessel function of the first kind, $\kappa_c = \alpha(1-\mathrm{i})/\sqrt{2}$ and $\mathrm{i} = \sqrt{-1}$. The axial flow rate is

$$Q^* = \tfrac{1}{2}\omega V_T \sin(\omega t_c^* + \varphi) = 2\pi\omega L_T b^2 \int_0^{R_c} w_c r_c \, \mathrm{d}r_c. \tag{24}$$

The pressure gradient function amplitude, B, in (5) is then obtained by substituting (23) into (24). Representing the core variables in terms of the film variables, (i.e. $r_c = (1-\varepsilon)^{-1} r$, $z_c = \delta(1-\varepsilon)^{-1} z$, $t_c = \Omega t$, $R_c = (1-\varepsilon)^{-1} R_w$, $p_c = \delta\varepsilon^{-2}\gamma^{-1}\Omega^{-1}\lambda^{-1} p_f$, $u_c = \varepsilon\delta^{-1}(1-\delta)^{-1}\Omega^{-1}\lambda^{-1} u_f$, $w_c = (1-\varepsilon)^{-1}\Omega^{-1}\lambda^{-1} w_f$), we find that the core pressure gradient (see (15) and (22)) is

$$\frac{\partial p_c}{\partial z} = \alpha^2 \frac{\varepsilon}{(1-\varepsilon)^4} Ca \hat{B}(z) \sin \Omega t,$$

$$\hat{B}(z) = \tfrac{1}{4}\left|\tfrac{1}{2}\mathrm{i}R_w^2 + \frac{(1-\mathrm{i})}{\sqrt{2}}\frac{(1-\varepsilon)}{\alpha} R_w \frac{J_1(\kappa R_w)}{J_0(\kappa R_w)}\right|^{-1}, \tag{25}$$

where $B = (\alpha^2/(1-\varepsilon)^2)\hat{B}$, $\kappa = 2^{-1/2}(1-\mathrm{i})(1-\varepsilon)^{-1}\alpha$ is proportional to the Womersley number, and p_c is now scaled in terms of the film pressure scale. Here, J_1 is the order-one Bessel function of the first kind. The shear stress at the wall surface is then

$$\tau = -\frac{\partial w}{\partial y} = \alpha \frac{Ca}{(1-\varepsilon)^2} \mathrm{Re}\left(\hat{B}(z)\frac{J_1(\kappa R_w)}{J_0(\kappa R_w)}\exp(\mathrm{i}(\Omega t - \pi/4))\right). \tag{26}$$

The shear stress amplitude also depends on the quantity $B(z)(J_1(\kappa R_w)/J_0(\kappa R_w))$ which increases as the core radius R_w decreases. In the limit $\Omega \gg 1$, the core radius R_w that appears in the expressions for the core pressure gradient in (25) and shear stress in (26) can effectively be replaced by $R(z,t) = 1 - \varepsilon + \varepsilon h(z,t)$, a function of the slower capillary time t. Expressions for p_c and τ can then be substituted into the interfacial boundary conditions, equations (14) and (15), and then inserted into the kinematic boundary condition, equation (22).

4. Unperturbed linear stability

At early times, the deviation of the film thickness from its uniform state is small. The evolution equation for h, equation (22) can be linearized, yielding

$$\frac{\partial h}{\partial t} + \tfrac{1}{3}\left(\frac{\partial^2 h}{\partial z^2} + \frac{\partial^4 h}{\partial z^4}\right) + A\sin(\Omega t + \varphi)\frac{\partial h}{\partial z} = 0, \tag{27}$$

where A is a constant obtained from the linearization of the core shear stress. The shear stress term does not affect linear stability since it can be eliminated from (27) by making a coordinate transformation of the form $Z = z + (A/\Omega)\cos(\Omega t + \varphi)$, $T = t$. A normal mode analysis is carried out by letting $h(Z,t) = C(\exp(gt + \mathrm{i}kZ))$, where $C \ll 1$ is the amplitude of an infinitesimal disturbance, g is the growth rate and k is the wavenumber. Substituting this into the linearized evolution equation yields

the classical dispersion equation $g = k^2(1 - k^2)/3$ for no base flow as in Hammond (1983). Disturbances grow with time provided that $0 < k < 1$, and decay if $k > 1$. The maximum growth rate occurs at $k = 2^{1/2}$.

5. Results

The evolution equation derived in § 3, equation (22), together with the expressions for the core shear stress, (26), and normal stress, (15) and (25), is solved numerically using the method of lines (Halpern & Grotberg 1992) subject to periodic boundary conditions and a sinusoidal initial condition with an amplitude that is 1% of the unperturbed film thickness parameter ε, and the wavelength being the most dangerous one according to the linear stability theory described above. The length of the computational domain is equal to this most dangerous wavelength.

Some of the parameter values that have been selected in this paper were motivated by our previous work on pulmonary airway closure (Halpern & Grotberg 1992), but we consider parameter values that are also pertinent to other small-scale multiphase flows in porous media involving thin films coating cylindrical tubes (Gauglitz & Radke 1988). Gauglitz & Radke (1988) predicted a critical value of $\varepsilon = 0.12$ for liquid plug formation in a tube whose length is equal to the most dangerous wavelength based on linear stability theory. In all of our computations $\varepsilon = 0.13$, a value just above the plug formation threshold for the zero-frequency case. Note that for this value of ε, the lubrication theory approximation becomes invalid as the core radius approaches 0. Johnson *et al.* (1991) demonstrated that their one-dimensional model for the deflection of the interface compared favourably with the numerical simulation of the full equations for film thicknesses outside the range of validity of lubrication theory ($\varepsilon = 0.2$) until just before meniscus formation occurred, suggesting that their one-dimensional evolution equation could accurately predict when closure occurs. Our computations were stopped before the core radius reached zero, and before inertia terms in the film became important.

A reference stroke length parameter value of $\lambda = 7.43$ was selected based on a tube of radius $a = 0.03\,\mathrm{cm}$ (corresponding to airway generation 15), and a tidal volume $V_T = 0.0006\,\mathrm{cm}^3$. For the majority of computations, we chose the viscosity of the film to be ten times that of water, so that $\mu_f = 0.1$ poise, while for the core we chose $\mu_c = 0.00018$ poise and $\nu_c = 0.15\,\mathrm{cm}^2\,\mathrm{s}^{-1}$, the dynamic and kinematic viscosities of air, respectively. Below we also provide some results with different viscosity ratios that are appropriate for liquid–liquid core–annular configurations. The surface tension of the interface is chosen to be 25 dynes cm^{-1} (Frerking *et al.* 2001).

The dimensional frequency ω appears in three of our five parameters. For the purposes of demonstrating the effects of changing ω, it is more convenient to represent the frequency-related parameters as $\alpha^2 = \varepsilon^3(1 - \varepsilon)\beta\Omega$, and $Ca = \varepsilon(1 - \varepsilon)\gamma\lambda\Omega$ where $\beta = \sigma b/(\mu_f \nu_c)$ and $\gamma = \mu_c/\mu_f$. Now all frequency information is carried in Ω. Recall that the model is valid for high frequencies. A reference frequency of 15 Hz is chosen corresponding to $\Omega = 5$.

Figure 3 shows a plot of the minimum core radius, $r_{min}(t)$, which corresponds to the maximum film thickness. The graph is for different dimensional frequencies $10\,\mathrm{Hz} \leqslant f \leqslant 25\,\mathrm{Hz}$ (corresponding to different Ω, α and Ca) and stroke length $\lambda = 14.86$. Consistent with the linear stability theory presented above, the initial decrease in $r_{min}(t)$ is independent of frequency, and the effect of the core flow only manifests itself when the film is sufficiently thick. For the zero-frequency case, tube occlusion occurs, i.e. the minimum core radius tends to zero in finite time, if $\varepsilon > 0.12$. As ω

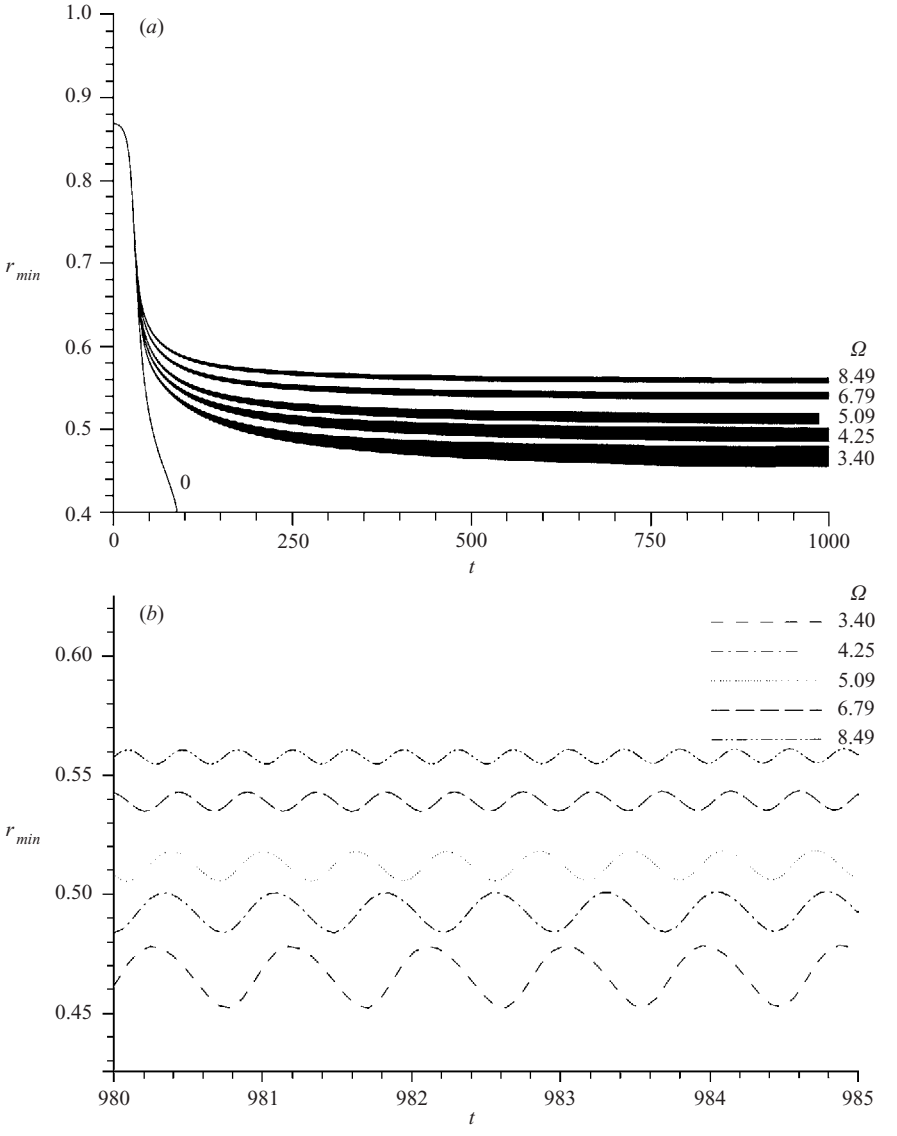

FIGURE 3. The effect of frequency on the minimum core radius, $r_{min}(t)$, with time t. Here, $\beta = 43.05$, $\varepsilon = 0.13$, $\gamma = 0.0018$ and $\lambda = 14.86$.

is increased, the onset of occlusion is delayed, and at some critical frequency the minimum core radius stabilizes about some non-zero mean value. Figure 3(*b*) shows the time-asymptotic profiles of $r_{min}(t)$ for frequencies that prevent occlusion. As ω increases, the mean value of $r_{min}(t)$ increases and the fluctuations around the mean decrease. Occlusion is also delayed and prevented by increasing the tidal volume (corresponding to different λ and Ca), as shown in figure 4, where $r_{min}(t)$ is plotted for different values of λ with $\Omega = 5.094$ and $\alpha = 0.74$.

The effect of core viscosity μ_c on $r_{min}(t)$ is shown in figure 5(*a*) with the frequency set at 15 Hz. Curve (i) corresponds to an air–liquid system as shown in figure 3, while the curves (ii) and (iii) are for liquid–liquid systems with identical densities

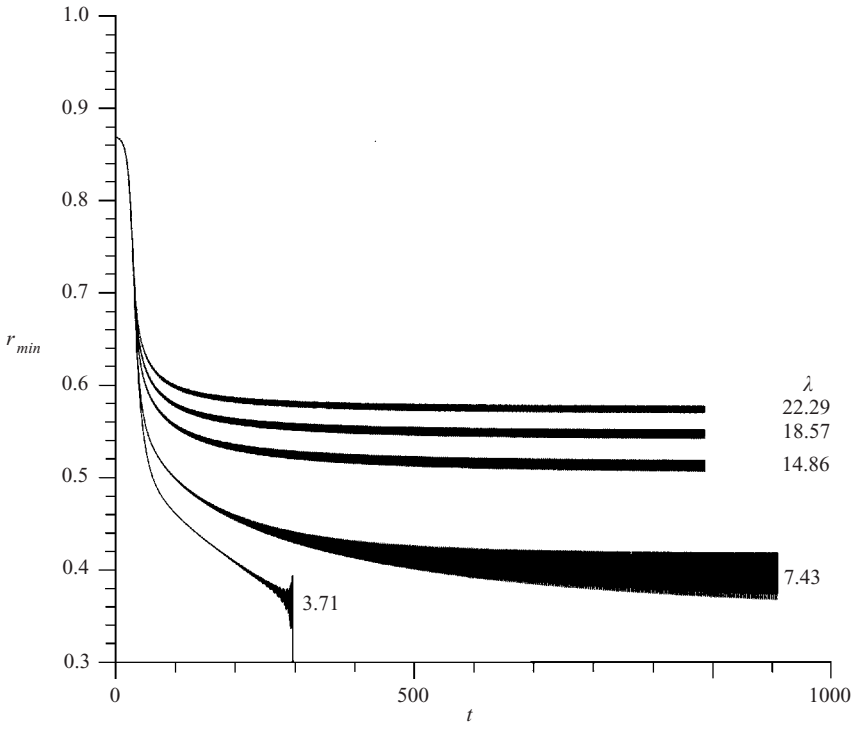

FIGURE 4. The effect of stroke length on the minimum core radius, $r_{min}(t)$, with time t. Here, $\alpha = 0.74$, $\varepsilon = 0.13$, $\gamma = 0.0018$ and $\Omega = 5.094$.

($\rho_c = 1\,\mathrm{g\,cm^{-3}}$). The film viscosities are the same for all three cases, $\mu_c = 0.1$ Poise. Since $Ca \propto \mu_c$ and $\alpha \propto \mu_c^{-1/2}$, increasing the core viscosity causes an increase in the shear stress amplitude (see equation (26)), which is more stabilizing since, as shown in figure 5(a), $r_{min}(t)$ tends to a larger cycle averaged value at large times.

The effect of film viscosity μ_f on $r_{min}(t)$ is shown in figure 5(b). Note that increasing the film viscosity and keeping all other system parameters fixed, results in an increase in Ω ($= Ca/(\gamma\lambda\varepsilon(1-\varepsilon))$) since the film time scale becomes longer compared with that of the core, but the core shear amplitude in (26) remains unchanged since it depends on α and Ca. Also, recall that time is scaled on $a\mu_f/\varepsilon^3\sigma$. At early times, the r_{min} decreases less rapidly for the more viscous case because of the larger film time scale; but the destabilizing effect of curvature becomes more dominant for the more viscous case since as Ω increases the film has less time to respond to the oscillatory core forcing.

An illustration of how the film thickness varies spatially over half an oscillation period is shown in figure 6. This case exhibits prevention of liquid plug formation by the oscillatory shear stress once the system has reached its time asymptotic state, with $\varepsilon = 0.13$, $\lambda = 14.86$, $Ca = 0.018$, $\alpha = 0.744$ and $\Omega = 5.094$. During the half-cycle shown for times $t = t_0 + m\pi/4\Omega$, the liquid bulge moves from left to right with a small capillary wave ahead of it. Behind the advancing bulge, the film thickness decreases monotonically. At this bulge speed, however, the trailing film is thicker than the precursor film, so the bulge volume diminishes as shown by an increasing r_{min} for $m = 1, 2$ and 3. The difference between the trailing and precursor films depends on how they are characterized. Suppose, without loss of generality, we define the regions

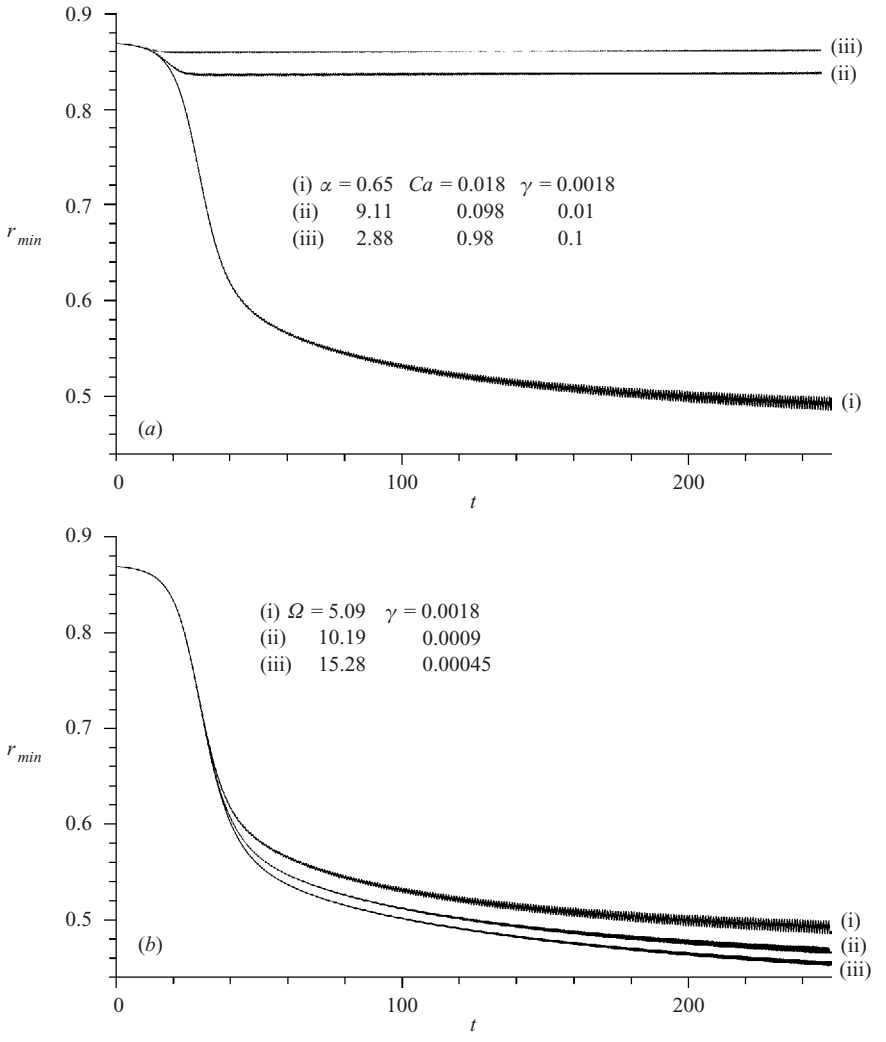

FIGURE 5. (*a*) The effect of film viscosity on the minimum core radius, $r_{min}(t)$, with time t. Here, $\varepsilon = 0.13$, $\lambda = 14.86$ and $\Omega = 5.094$; (*b*) The effect of core viscosity on the minimum core radius, $r_{min}(t)$, with time t. Here, $\varepsilon = 0.13$, $\lambda = 14.86$, $Ca = 0.018$, and the other parameters are as shown in the figure.

occupied by the trailing and precursor films by the two disconnected regions of the film where $0.9 \leqslant R(z, t) \leqslant 1$, then the trailing film is thicker (or its volume is larger) than the precursor film, as shown in figure 6 for $m = 4$. During the turnaround process, the bulge gains fluid from the film owing to the destabilizing azimuthal component of surface curvature in the face of a smaller shear perturbation. The bulge then starts moving back to the left, and the process repeats itself, except that the capillary wave is now on the left-hand side. The instantaneous streamlines in the film corresponding to the same times in the cycle displayed in figure 6 are shown in figure 7. As the bulge starts to move from left to right as shown in figure 7(*a*), there is a main clockwise vortex in the bulge as well as smaller, neighbouring vortical structures. However, at $m = 2$ (figure 7*c*) the main vortex has reversed direction, along with its neighbours.

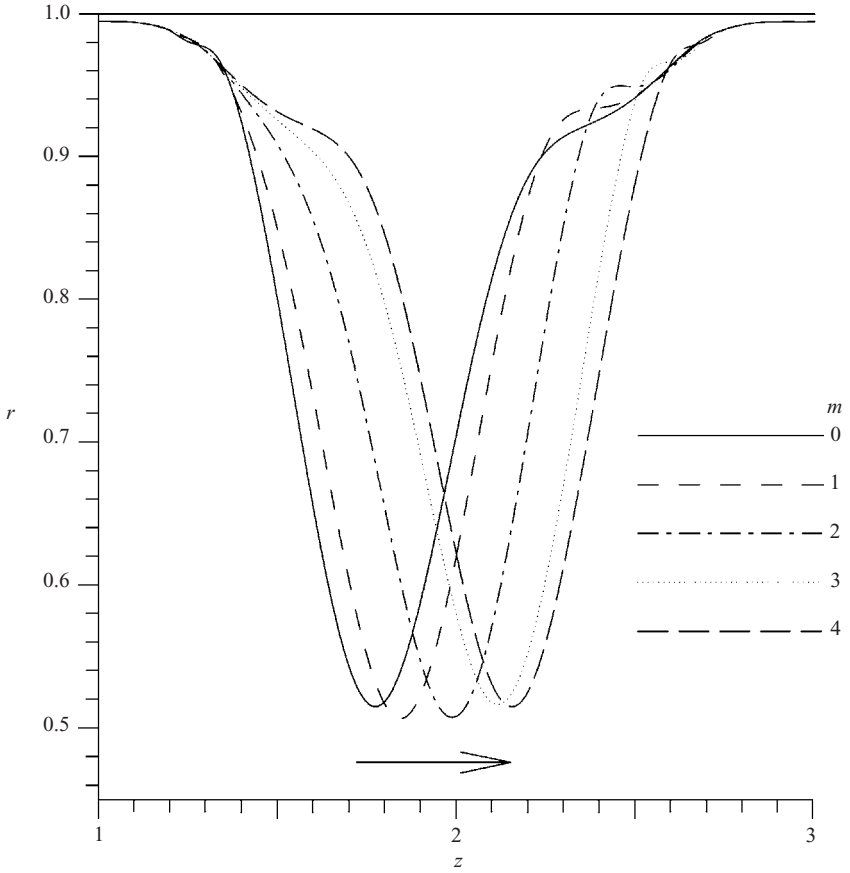

FIGURE 6. The shape of the airway–liquid interface, $1-\varepsilon+\varepsilon h(z,t)$ at $t=t_0+\pi m/4\Omega$, where $t_0=986.7228$, $\Omega=5.094$, $\varepsilon=0.13$, $\lambda=14.86$ and $0\leqslant m\leqslant 4$.

By this time, the core shear stress is strong enough to entrain the bulge fluid and dictate the vortex direction.

To assess whether closure occurs or not, we compute the square of the difference in film shape between two successive periods:

$$E=\int_0^L [R(z,t_0)-R(z,t_0+2\pi)]^2\,\mathrm{d}z, \tag{28}$$

where $t_0=n\pi$. Plug formation does not occur if $E\to 0$ as $t_0\to\infty$. Computationally, we stipulate that closure does not occur if E falls below a certain small tolerance (chosen here to be 10^{-6}) and remains below this tolerance value after a sufficiently large number of oscillations. In figure 8, the critical frequency above which plug formation does not occur, Ω_c, is plotted versus λ for $\varepsilon=0.13$. For the zero-frequency case, it is well known that increasing the unperturbed film thickness makes the system more unstable by enhancing the effect of the azimuthal component of curvature. For fixed ε the critical frequency increases with decreasing λ.

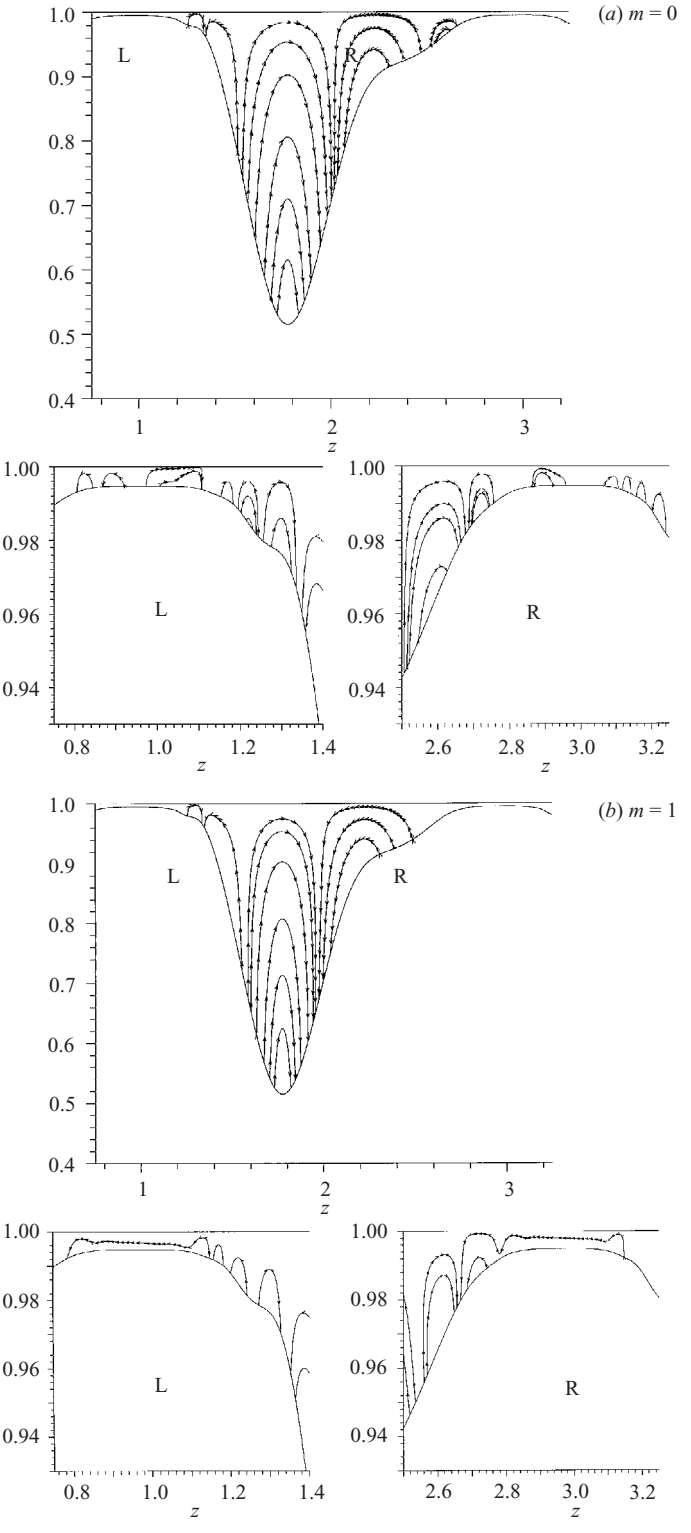

FIGURE 7(*a*, *b*). For caption see page 267.

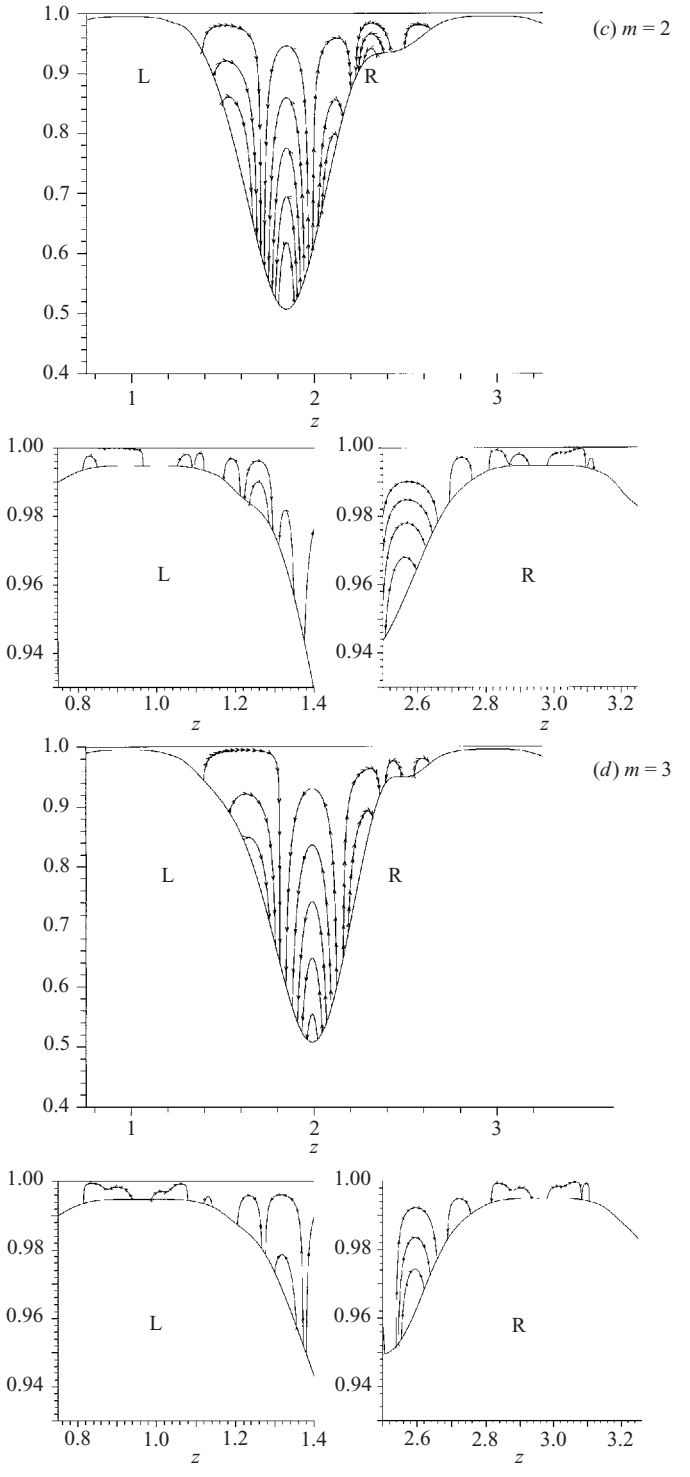

FIGURE 7(c, d). For caption see facing page.

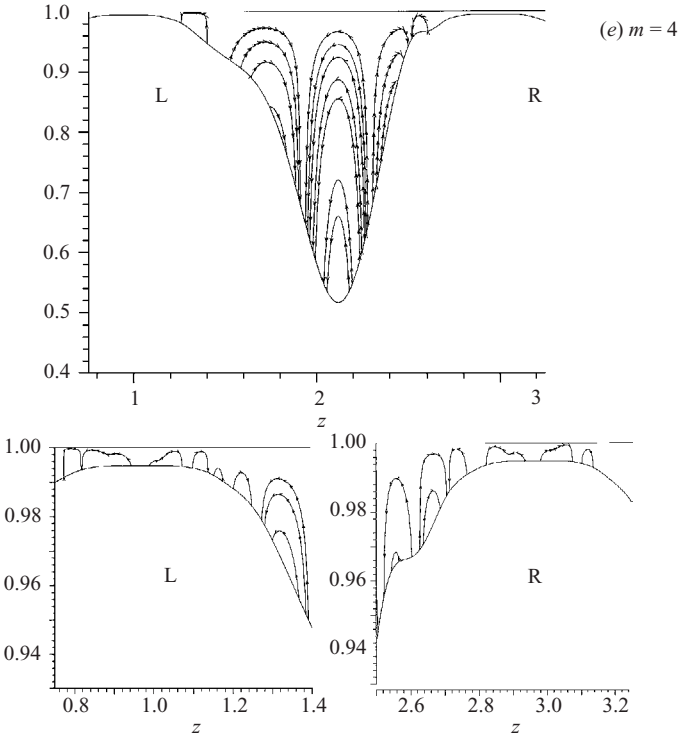

FIGURE 7. The shape of the air–liquid interface and instantaneous streamlines at $t = t_0 + \pi m/4\Omega$, where $t_0 = 986.7228$, $\Omega = 5.094$, $\varepsilon = 0.13$, $\lambda = 14.86$ and $0 \leqslant m \leqslant 4$. Inserts are shown in each graph to give an enlarged view of the thin film region.

6. Discussion

We have presented a model for the stability of a thin film coating the inner surface of a rigid cylindrical tube that includes the effects of an oscillatory air (core) flow which exerts tangential and normal stresses on the air–liquid interface. As in previous models that examine the stability of thin films with a passive core phase (Gauglitz & Radke 1988; Johnson *et al.* 1991; Halpern & Grotberg 1992), lubrication theory is used to derive an evolution equation for the position of the air–liquid interface which incorporates a more accurate representation for the interfacial curvature valid for thick films. The core flow is determined independently of the film flow by assuming that the core perceives the highly viscous film as a rigid boundary. This requires that the velocity scale for the core flow be larger than that for the thin film, implying that the product of the frequency parameter and the stroke length be much larger than unity. For smaller frequencies or tidal volumes, the fully coupled problem would have to be solved. However, our primary goal was to show that an oscillatory core flow could prevent plug formation.

As indicated by linear stability, the Rayleigh instability (Plateau 1873; Rayleigh 1892*a*; *b*) plays an initial role in creating the film's liquid bulge. The effect of the core on the film becomes important once the film is sufficiently thick. As the bulge is dragged across the domain by the core shear, there is a net loss in volume as it picks up less fluid from the film ahead of it than it loses to the film behind it, and therefore the minimum core radius increases and the bulge diminishes. During the turnaround

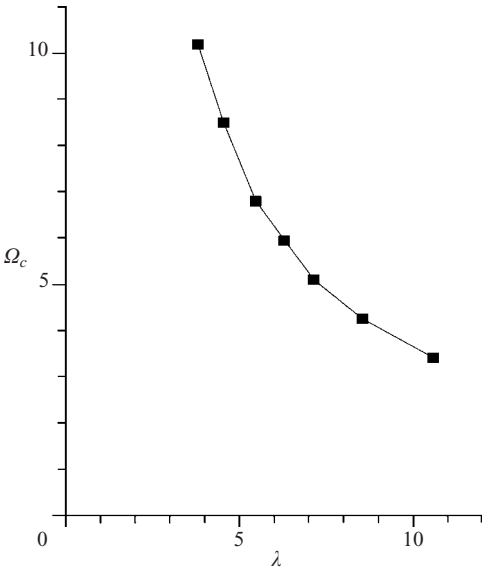

FIGURE 8. Critical frequency Ω_c versus stroke length for $\varepsilon = 0.13$.

process, capillarity is stronger than the shear stress and the bulge grows back and can then be reapplied to the wall with the reverse stroke. Indeed, we can think of this mechanism as a reversing butter knife, continuously reapplying the bulge fluid to the wall. When the process is tuned correctly, the two phases balance and there is no net growth of the liquid bulge over one cycle. Note that the changes in the bulge height are small because our model applies only for large Ω, and a large core capillary number Ca is required for saturation of the instability so that a large enough shear stress is impinged on the interface. Figures 3, 4 and 5(a) show that an increase in Ca, either due to an increase in ωL_T or μ_c, is stabilizing.

As mentioned above, the primary instability in the core–annular problem is due to the transverse component of curvature that appears in the normal stress condition. Other types of instability, such as the Rayleigh–Taylor instability can, in some limits, be described by a similar type of equation as those used to describe CAFs (see for example, Halpern & Frenkel 2001). Halpern & Frenkel (2001) examined the effect of an oscillating Couette flow on the gravitational Rayleigh–Taylor instability, where two viscous fluids of different densities are sheared between two oscillating parallel plates. It was demonstrated that the lighter fluid coating the bottom plate would not be ruptured by the heavier layer, provided the interfacial shear stress was strong enough. Our governing equation for the film deflection, equation (22), reduces to their weakly nonlinear Kuramoto–Sivashinsky equation for small interfacial deflections in the limit of small α but very large Ca, with $\tau = \alpha^2\ Ca \sin \Omega t$. One main difference, however, is that in our model the frequency appears in α, Ca and Ω, so that higher shears are generated at high frequencies. In Halpern & Frenkel (2001), the shear amplitude and frequency were not coupled, and it was shown that film rupture could occur at high frequencies.

Pulmonary airway closure can occur in the small airways of the lung as a result of liquid plug formation due to the capillary instability (Halpern & Grotberg 1992). However, surfactant is normally present at the air–liquid interface which tends to

reduce the surface tension and induce a Marangoni shear force that delays or prevents closure from occurring for the passive core case (Halpern & Grotberg 1993*a*; Otis *et al.* 1993). Frenkel & Halpern (2002) have shown that the presence of surfactant in a two-fluid shear flow can be linearly destabilizing. Therefore, it would be interesting to consider the effects of surfactant on the current model.

We would like to thank Dr Julie A. Moriarty. This work was supported by NASA Grants NAG3-2196 and NAG3-2740, and NSF Grants BES-9820967, CTS-9412523, CTS-9896217 and DMS-0079478, and NIH Grant HL-41126.

REFERENCES

Aul, R. W. & Olbricht, W. L. 1990 Stability of a thin annular film in pressure-driven, low-Reynolds number flow through a capillary. *J. Fluid Mech.* **215**, 585–599.

Cassidy, K. J., Halpern, D., Ressler, B. G. & Grotberg, J. B. 1999 Surfactant effects in model airway closure experiments. *J. Appl. Physiol.* **87**, 415–427.

Chen, K. 1991 Interfacial instability due to elastic stratification in concentric co-extrusion of two viscoelastic fluids. *J. Non-Newtonian Fluid Mech.* **40**, 155–175.

Coward, A. V. & Papageorgiou, D. T. 1994 Stability of oscillatory two-phase Couette flow. *IMA J. Appl. Maths* **55**, 75–93.

Coward, A. V., Papageorgiou, D. T. & Smyrlis, Y. S. 1995 Nonlinear stability of oscillatory core–annular flow: a generalized Kuramoto–Sivashinsky equation with time periodic coefficients. *Z. angew. Math. Phys.* **46**, 1–39.

Edo, H., Kimura, H., Niijima, M., Sakabe, H., Shibuya, M., Kanamaru, A., Homma, I. & Kuriyama, T. 1998 Effects of chest wall vibration on breathlessness during hypercapnic ventilatory response. *J. Appl. Physiol.* **84**, 1487–1491.

Frenkel, A. & Kerchman, V. I. 1994 On large amplitude waves in core–annular flows. *14th IMACS World Congress on Computations and Applied Mathematics, Atlanta, GA, July 11–15* (ed. W. F. Ames), vol. 2, pp. 379–400.

Frenkel, A. L., Babchin, A. J., Levich, B. G., Shlang, T. & Sivashinsky, G. I. 1987 Annular flow can keep unstable flow from breakup: nonlinear saturation of capillary instability. *J. Colloid Interface Sci.* **115**, 225–233.

Frenkel, A. L. & Halpern, D. 2002 Stokes-flow instability due to interfacial surfactant. *Phys. Fluids* **14**, L45–L48.

Frerking, I., Gunther, A., Seeger, W. & Pison, U. 2001 Pulmonary surfactant: functions, abnormalities and therapeutic options. *Intens. Care Med.* **27**, 1699–1717.

Gauglitz, P. A. & Radke, C. J. 1988 An extended evolution equation for liquid film breakup in cylindrical capillaries. *Chem. Engng Sci.* **43**, 1457–1465.

Goren, S. L. 1962 The instability of an annular thread of fluid. *J. Fluid Mech.* **12**, 309–319.

Graham, D. R. & Higdon, J. J. L. 2002 Oscillatory forcing of flow through porous media. Part 1. Steady flow. *J. Fluid Mech.* **465**, 213–235.

Halpern, D. & Frenkel, A. L. 2001 Saturated Rayleigh–Taylor instability of an oscillating Couette film flow. *J. Fluid Mech.* **446**, 67–93.

Halpern, D. & Grotberg, J. B. 1992 Fluid-elastic instabilities of liquid-lined flexible tubes. *J. Fluid Mech.* **244**, 615–632.

Halpern, D. & Grotberg, J. B. 1993*a* Surface tension instabilities of liquid-lined elastic tubes. In *Contemporary Mathematics (Fluid Dynamics in Biology)*, vol. 141, pp. 295–316. American Mathematical Society.

Halpern, D. & Grotberg, J. B. 1993*b* Surfactant effects on fluid-elastic instabilities of liquid-lined flexible tubes: a model of airway closure. *J. Biomech. Engng* **115**, 271–277.

Hammond, P. S. 1983 Nonlinear adjustment of a thin annular film of viscous fluid surrounding a thread of another within a circular pipe. *J. Fluid Mech.* **137**, 363–384.

Hughes, J. M. B., Rosenzweig, D. Y. & Kivitz, P. B. 1970 Site of airway closure in excised dog lungs: histologic demonstration. *J. Appl. Physiol.* **29**, 340–344.

Isayev, A. I., Wong, C. M. & Zeng, X. 1990 Flow of thermoplastics in an annular die under orthogonal oscillations. *J. Non-Newtonian Fluid Mech.* **34**, 375–397.

Johnson, M., Kamm, R. D., Ho, L. W., Shapiro, A. & Pedley, T. J. 1991 The nonlinear growth of surface-tension-driven instabilities of a thin annular film. *J. Fluid Mech.* **233**, 141–156.

Joseph, D. D. & Renardy, Y. 1991 *Fundamentals of Two- Fluid Dynamics, Vol. I: Mathematical Theory and Application; Vol. II.- Lubricated Transport, Drops, and Miscible Liquid*. Springer.

Kerchman, V. I. & Frenkel, A. L. 1994 Interaction of coherent structures in a film flow: simulations of a highly nonlinear evolution equation. *Theor. Comput. Fluid Dyn.* **6**, 235–254.

Kouris, C. & Tsamopoulos, J. 2001*a* Core–annular flow in a periodically constricted circular tube. Part 1. Steady-state, linear stability and energy analysis. *J. Fluid Mech.* **432**, 31–68.

Kouris, C. & Tsamopoulos, J. 2001*b* Dynamics of axisymmetric core–annular flow in a straight tube. I. The more viscous fluid in the core, bamboo waves. *Phys. Fluids* **13**, 841–858.

Kouris, C. & Tsamopoulos, J. 2002 Dynamics of the axisymmetric core–annular flow. II. The less viscous fluid in the core, saw tooth waves. *Phys. Fluids* **14**, 1011–1029.

Macklem, P. T., Proctor, D. F. & Hogg, J. C. 1970 The stability of peripheral airways. *Respir. Physiol.* **8**, 191–203.

Melli, T. R., Desantos, J. M., Kolb, W. B. & Scriven, L. E. 1990 Cocurrent downflow in networks of passages – microscale roots of macroscale flow regimes. *Indust. Engng Chem. Res.* **29**, 2367–2379.

Otis, D. R., Jr, Johnson, M., Pedley, T. J. & Kamm, R. D. 1993 Role of pulmonary surfactant in airway closure: a computational study. *J. Appl. Physiol.* **75**, 1323–1333.

Plateau, J. A. F. 1873 *Statique experimentale et theorique des liquides soumis aux seules forces moleculaires*. Gauthier-Villars.

Rayleigh, lord 1892*a* On the instability of a cylinder of viscous liquid under capillary force. *Phil. Mag.* **34**, 145.

Rayleigh, lord 1892*b* On the instability of cylindrical fluid surfaces. *Phil. Mag.* **34**, 177–180.

Wei, H. H. & Rumschitzki, D. S. 2002*a* The linear stability of a core–annular flow in an asymptotically corrugated tube. *J. Fluid Mech.* **466**, 113–147.

Wei, H. H. & Rumschitzki, D. S. 2002*b* The weakly nonlinear interfacial stability of a core–annular flow in a corrugated tube. *J. Fluid Mech.* **466**, 149–177.

Wong, C. M., Chen, C. H. & Isayev, A. I. 1990 Flow of thermoplastics in an annular die under parallel oscillations. *Polymer Engng Sci.* **30**, 1574–1584.

Yih, C.-S. 1967 Instability due to viscosity stratification. *J. Fluid Mech.* **27**, 337–352.